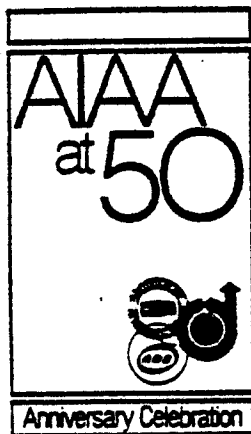


**AIAA-82-0202**

**TOPEX Orbit Sustenance Maneuver Design**

J.A. Kechichian, Jet Propulsion Lab.,  
Pasadena, CA



**AIAA 20th Aerospace  
Sciences Meeting**

January 11-14, 1982/Orlando, Florida

## TOPEX ORBIT SUSTENANCE MANEUVER DESIGN

J. A. Kechichian\* \*\*  
Jet Propulsion Laboratory, California Institute of Technology  
Pasadena, California

### Abstract

A trade-off analysis between maneuver period, execution errors, and orbit determination uncertainties is carried out for the Ocean Topography Experiment (TOPEX) spacecraft for a given nodal equatorial constraint. Semimajor axis and eccentricity are controlled with minimum impulse using the linear theory of optimal transfer between close coplanar near-circular orbits. Ellipses of equal minimum and average maneuver periods are presented in the  $(3\sigma_{ex}, 3\sigma_{pp})$  space for different nodal equatorial constraints enabling the determination of the appropriate combination of execution errors and orbit determination uncertainties that guarantees a mission required minimum maneuver period for a given nodal deadband.

### I. Introduction

The Ocean Topography Experiment (TOPEX) is a proposed NASA earth satellite mission to study the general circulation of the oceans by means of on-board precision altimeter measurements. The Jet Propulsion Laboratory has performed preliminary (Phase A) conceptual studies of the TOPEX mission. This paper describes one aspect of these studies, the TOPEX orbit sustenance maneuver design.

The orbit selected by the mission design specialists has a mean altitude of 1334 km and is inclined  $63^\circ$  relative to the equator. This orbit is not strongly influenced by atmospheric drag nor synchronous with the dominant tidal constituents and can observe almost all the open water on Earth, in order to resolve the two components of geostrophic current at mid-latitudes. Furthermore, in order to sample the ocean variability without ambiguity, the satellite's ground track was designed to repeat itself almost exactly every ten days. However, the node at the equator experiences an appreciable drift which is mainly due to atmospheric drag which decays the orbit semimajor axis and to the perturbing effects of the Earth gravity harmonics, soli-lunar attraction, and solar radiation pressure.

The scientific personnel require to maintain the longitude of the spacecraft's initial ascending node within a narrow deadband of  $\pm 1$  km at the equator, and this is accomplished by way of maneuvers whose frequency should not exceed once per month, in order to simplify mission operations and reduce interference with science.

The rate and pattern of the nodal drift are a strong function of the orbit's semimajor axis

\* Member AIAA

\*\* Member of Technical Staff, Future Missions Studies

Released to AIAA to publish in all forms.

Copyright © American Institute of Aeronautics and Astronautics, Inc., 1982. All rights reserved.

which must be controlled very tightly if the above requirement is to be satisfied.

The maneuver strategy consists, therefore, of transferring the spacecraft to an orbit whose semi-major axis is such that the nodal constraint boundaries are not violated for the longest possible time, maximizing thereby the interval between maneuvers. These maneuvers are computed using Contensou's linear theory of optimal transfer between close coplanar near-circular orbits in which both a (semimajor axis) and  $\bar{e}$  (eccentricity vector) are controlled with minimum impulse. These transfers introduce execution errors and are dependent on the orbit determination uncertainties on the semimajor axis.

The execution errors are mainly due to cutoff errors and to hot-cold firings of the propulsion system, while the errors in the estimates of the position and velocity of the spacecraft in its orbit are influenced by errors in the measurement of the spacecraft's position and the errors in estimating the perturbing forces acting on it. The uncertainty in the knowledge of the gravitational field and the inability to know the precise location of the tracking stations relative to the center of the Earth, are among the main sources of orbit determination uncertainties.

It is, therefore, necessary to minimize  $\sigma_{ex}$  and  $\sigma_{\Delta a}$ , which are respectively the execution error and the uncertainty on the semimajor axis, in order to maximize the interval between maneuvers; this, in effect, constitutes a tradeoff analysis between maneuver period and  $\sigma_{ex}$ ,  $\sigma_{\Delta a}$ .

The targeting strategy takes advantage of the fact that atmospheric drag forces the node to drift eventually towards larger values, even if it is drifting initially in the opposite direction for a biased semimajor axis. This, in effect, makes it possible to position the spacecraft on the right end of the deadband ( $+1$  km) and chose its semimajor axis in such a way that the corresponding ground track drifts initially towards the other end without violating it, before reversing the motion to the right and violating it after the longest possible time.

However, this target orbit cannot be reached exactly because  $\sigma_{ex}$  and  $\sigma_{\Delta a}$  combine to create an overall uncertainty in the achieved semimajor axis. The numerical input to the trajectory generating programs used in this paper are as follows:

Mass of the spacecraft = 1000 kg  
Cross sectional area =  $10 \text{ m}^2$   
Sun and moon's fourth degree spherical harmonics included  
Coefficient of atmospheric drag  $C_D = 2.1$   
Solar radiation pressure force coefficient =  $-5.8 \cdot 10^{-4} \text{ (kg/hr}^2\text{)/km}$

Finally, Appendices A and B drawn from the lecture notes on space mechanics by Professor John

V. Breakwell of Stanford University describe the optimal transfer solutions and the error analysis used in the paper.

## II. Linear Analysis of the Nodal Drift at the Equator

The TOPEX baseline mean orbital elements borrowed from Reference 1 and listed below in Table 1 are average Kepler elements and are computed by Jet Propulsion Laboratory's SAMDP software using its long term orbit prediction option (LOP). These elements, based on a nominal launch time of 1430 GMT on 1 September 1986 from the Western Test Range (WTR), are obtained by integrating the Lagrange planetary equations for average elements. The gravitational disturbing functions are evaluated by analytical averaging while atmospheric drag and solar radiation pressure disturbing functions are evaluated by numerical averaging.

Table 1. TOPEX Baseline Mean Orbital Elements

$a$	= 7712.1903 km (semimajor axis)
$e$	= 0 (eccentricity)
$i$	= 63°.434949 (inclination)
$\Omega$	= 277°.67199 (right ascension of node)
$\omega$	= 0° (argument of periaipse)
$M$	= 0° (mean anomaly at epoch)

The mean equatorial altitude of this orbit is  $\bar{h} = 1334.05$  km with an Earth mean equatorial radius of  $R_e = 6378.14$  km. This orbit is an exact ten day repeat orbit covering 127 revolutions in that period of time and regaining the initial East longitude of its ascending node of  $\lambda = 90°.7091$  at the end of each such interval.

A parametric study can be carried out as a first approximation, in order to relate maneuver frequency as a function of the nodal drift at the equator for different levels of orbit determination uncertainties and maneuver execution errors.

Taking into account the effect of the second zonal harmonic  $J_2$ , the nodal period can be evaluated by

$$P_n = \frac{2\pi a^{3/2}}{\mu^{1/2}} \left[ 1 - \frac{3}{2} J_2 \left( \frac{R_e}{a} \right)^2 (4c_1^2 - 1) \right] \quad (2-1)$$

where  $a$  is the orbit semimajor axis,  $i$  its inclination respective to the equator, and  $\mu$  the Earth's gravitational constant. The rate of change of  $P_n$  with respect to  $a$ , is given by

$$\frac{\partial P_n}{\partial a} = 3\pi \left( \frac{a}{\mu} \right)^{1/2} \left[ 1 - \frac{3}{2} J_2 \left( \frac{R_e}{a} \right)^2 (4c_1^2 - 1) \right] + \frac{6\pi a^{-3/2}}{\mu^{1/2}} J_2 R_e^2 (4c_1^2 - 1) \quad (2-2)$$

The nodal period is essentially a function of  $a$  and with

$$\mu = 398601.3 \text{ km}^3/\text{s}^2$$

$$J_2 = 1.08263 \cdot 10^{-3}$$

$$\frac{\partial P_n}{\partial a} = 1.31125 \text{ s/km}$$

Equation (B-12) of Appendix B can now be used as follows

$$\begin{aligned} \delta a &= \frac{2}{n} \delta \dot{y} + 4\delta x \\ E\{\delta a\}^2 &= \frac{4}{n^2} E\{\delta \dot{y} \delta \dot{y}\} + \frac{8}{n} E\{\delta \dot{y} \delta x\} + 16E\{\delta x \delta x\} \\ \sigma_a^2 &= \frac{4}{n^2} \sigma_{\dot{y}}^2 + \frac{8}{n} \rho \sigma_x \sigma_{\dot{y}} + 16\sigma_x^2 \end{aligned} \quad (2-3)$$

where  $\rho$  is the correlation factor between  $\sigma_x$  and  $\sigma_{\dot{y}}$ . With respect to an inertial reference frame, the equator moves at a rate  $V_e = \omega_e R_e = .72921159 \cdot 10^{-4} \times 6378.14 = 465101361 \text{ km/s}$  and travels a distance  $D$  in time  $t = \frac{D}{V_e} = 2.15 D$  seconds.

This indicates that the subsatellite point on the surface of the Earth must reach the equator within  $\pm 2.15 D$  seconds from its nominal crossing time in order to satisfy the  $\pm D$  km nodal deadband at the equator.

Given  $\sigma_a$  from (2.3), and using the partial in (2.2),  $\delta P_n = \sigma_a \times 1.311 \text{ s/rev}$ , and a linear expression of the nodal drift is obtained by

$$d = \delta P_n \times V_e \times N \quad (2.4)$$

where  $N$  represents the number of revolutions flown by TOPEX in its exact ten day repeat orbit in a number of days equal to a multiple of ten.

Figure 1 shows the linear growth of  $d$  as a function of time for  $\sigma_x = 1$  meter and  $\sigma_{\dot{y}} = 1$  mm/s for both  $\rho = 0$  and  $\rho = -1$  (uncorrelated and fully correlated cases). For example, for a maneuver period of 30 days, the nodal drift is between .8 and 1 km with the upper bound corresponding to the uncorrelated case.

## III. A Preliminary Targeting Strategy for Nodal Drift Control

It is required to maintain the initial East longitude of the ascending node  $\lambda = 90°.7091$  within a tight deadband at the equator. There exists a circular Keplerian orbit of a given semimajor axis that repeats itself exactly after ten days and regains the initial East longitude of its ascending node at the end of each repeat cycle. This orbit is assumed to be under the influence of the second zonal  $J_2$  alone and its mean elements are shown in Table 1. When the perturbing effects of the other gravity harmonics (21 x 21 field), atmospheric drag, solar radiation pressure, and soli-lunar perturbations are taken into account, the orbit experiences an appreciable drift of its node at the equator and, therefore, cannot repeat itself exactly every ten days as before. This relatively small drift must be controlled by maneuvers at frequent intervals, in order to maintain the initial node within a small deadband of  $\pm 1$  km.

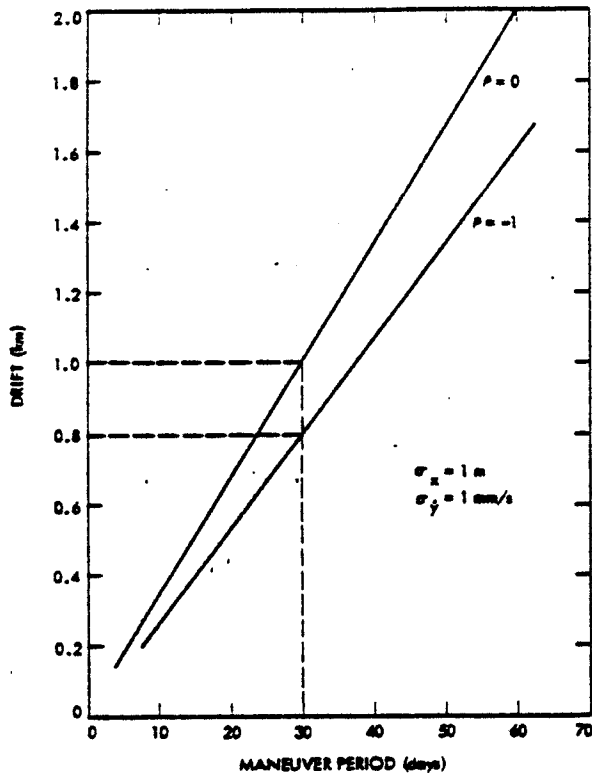


Figure 1. Maneuver Tradeoffs

Figure 2 shows how the nodal drift, plotted at ten day intervals, is a strong function of the initial semimajor axis. It is convenient to position the initial node at the +1 km end of the deadband, in order to allow it to drift initially towards the other end before turning and violating the deadband after the longest possible time. The

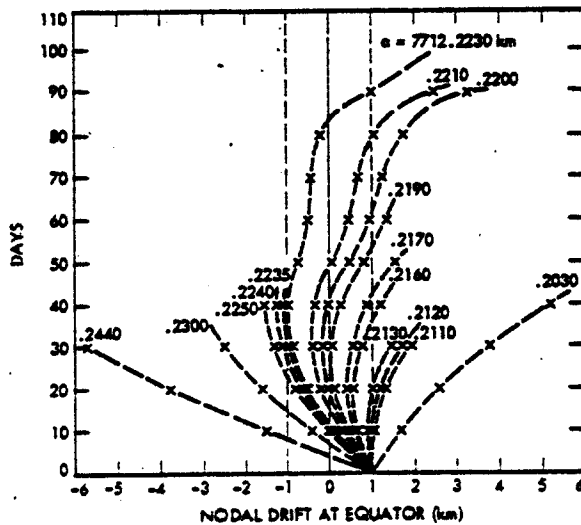


Figure 2. "S" Curves (right limit)  $\pm 1$  km Deadband

initial circular orbit of semimajor axis  $a = 7712.2230$  km is barely tangent to the -1 km end and stays for the longest period of 90 days inside the deadband. Orbits with smaller semimajor axis violate the deadband necessarily at the +1 km end while larger orbits violate the other end.

Figure 3 shows the nodal drift of this nominal orbit with all the above perturbations active, with third body perturbations turned off, and with drag turned off respectively. The strong influence of atmospheric drag is apparent in these plots; it is responsible for the drift of the node to the East because it decays semimajor axis even though the drift is initially to the West because of a small bias in semimajor axis. These orbits, which are relatively close to one another, experience the same linear eccentricity growth generated mainly by the Earth's  $J_{5,0}$  and  $J_{7,0}$  harmonics. This is displayed in Figure 4a, which also shows that the mission imposed constraint on the eccentricity  $e < .001$  is not violated until after 140 days. An additional maneuver is required at this point to circularize the orbit.

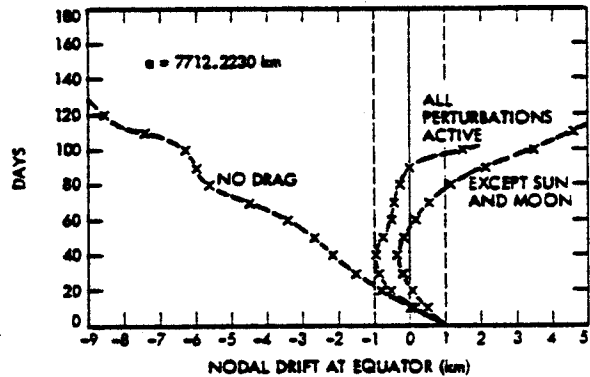


Figure 3. Effect of Perturbation of Nodal Drift

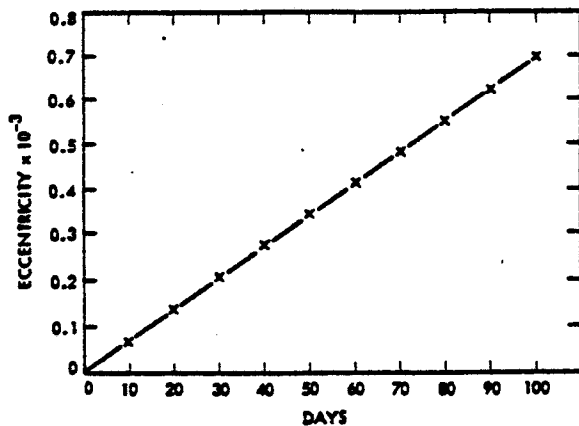


Figure 4a. Evolution of Eccentricity vs. Time

In Figure 4b, the nominal orbit drift pattern is shown as AFG; at point G, reached after some 90 days from A, the orbit can be retargeted to the circular orbit with nominal semimajor axis of 7712.2230 km to follow the path GHI and stay for another period of 90 days within the deadband.

However, the maneuvers introduce execution errors and the transfer parameters are dependent on the orbit determination uncertainties on the premaneuver semimajor axis. A fixed execution error of 1 mm/s introduces an error in the target semimajor axis of roughly  $\pm 4$  m; the two  $\Delta V$ 's that achieve the coplanar transfer (semimajor adjust and circulation) are computed from the solutions presented in Appendix A. The target orbit is, therefore, given by  $a = 7712.2230$  km and the lower bound  $a = 7712.2147$  km. Point B is reached in 30 days after A and corresponds to the worst achieved orbit, since it violates the deadband in the shortest time.

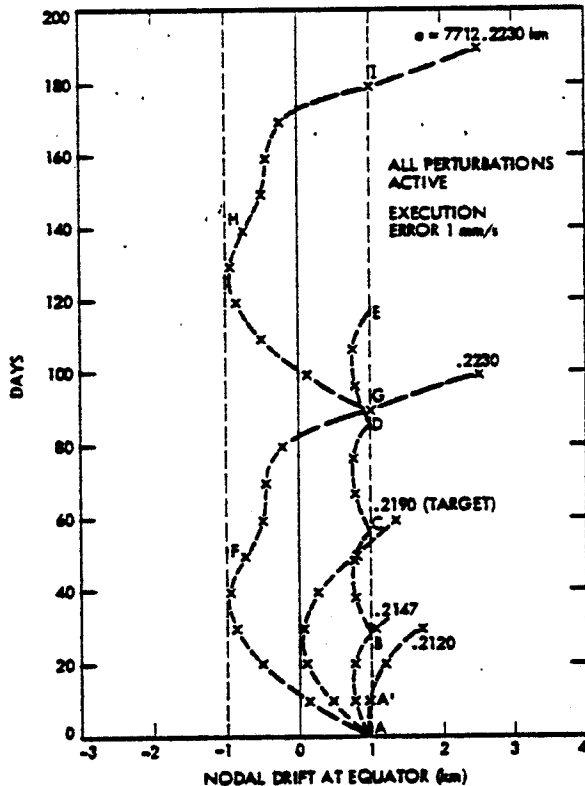


Figure 4b. Simple Maneuver Strategy

At B, a retargeting to 7712.2190 km will again produce a worst drift pattern given by BC and so on. If an orbit determination uncertainty of 2 m on the semimajor axis is taken into account and linearly combined with the previous 1 mm/s execution error, then the worst achievable orbit would be  $a = 7712.2120$  km shown by AA' in Figure 4b and would maintain its repeat node in the  $\pm 1$  km deadband for only 12 days. The advantage of this strategy is that the deadband is always violated at the  $+1$  km end, since it is not possible to achieve a semimajor axis higher than the nominal orbit. However, a clear disadvantage of this strategy is the small value of the minimum maneuver period of only 12 days that must be considered.

#### IV. Orbit Sustainance Maneuver Design: Right End Violation

In the last section, the target orbit was chosen in such a way that for a given maximum fixed

execution error on each of the two  $\Delta V$ 's achieving the required coplanar transfer, the largest achieved change in  $a$  would yield that particular orbit whose nodal crossing pattern at the equator would remain within the required constraint limits for the longest possible time.

The execution errors acting in the opposite direction would yield the smallest change in  $\Delta a$  and for small deadbands in the range of  $\pm 1$  km, it is the orbit with the smallest semimajor axis that violates the right side ( $+1$  km) of the deadband within a few days. This time is then chosen to represent the minimum maneuver period (worst case) from an execution error point of view.

If the target orbit semimajor axis is allowed to increase, the highest achieved  $\Delta a$  and the lowest achieved  $\Delta a$ , corresponding to the two extreme bounds on orbits, would reach a point where the left and right end constraints are violated simultaneously on the same day. This effectively increases appreciably the value of the minimum maneuver period without affecting its maximum value. The inverse problem of finding the corresponding fixed execution error must now be solved.

This strategy is best illustrated graphically by plotting the nodal drift at the equator of a series of neighboring circular orbits for different constraint values. Three such cases are considered ( $\pm 0.5$  km,  $\pm 1$  km, and  $\pm 2$  km) and shown in Figure 5, 2 and 6, respectively. For the  $\pm 0.5$  km deadband, the orbit corresponding to the largest maneuver period of 55 days has an initial semimajor axis of 7712.2193 km, while for the  $\pm 2$  km deadband, the circular orbit of initial  $a = 7712.2276$  km remains in that deadband for more than 125 days.

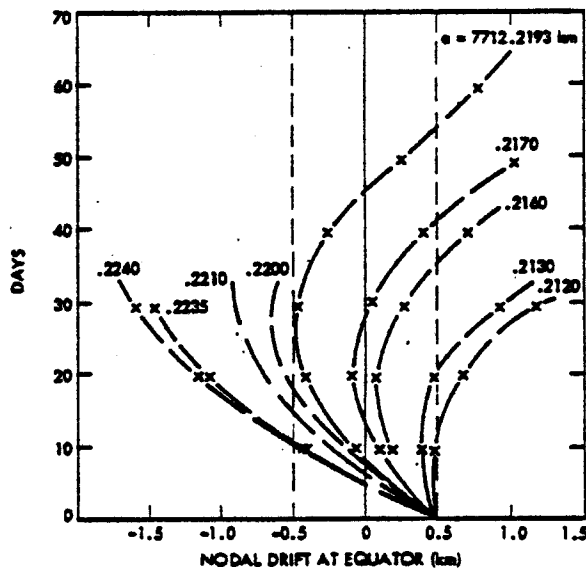


Figure 5. "S" Curves (right limit)  $\pm 5$  km Deadband

Each orbit violates the constraint once starting from small values of  $a$ , until the maximum period is reached by the orbit that is barely tangent to the left boundary. Figure 7 shows the evolution of the constraint boundary crossing time vs. initial semimajor axis. After the maximum time

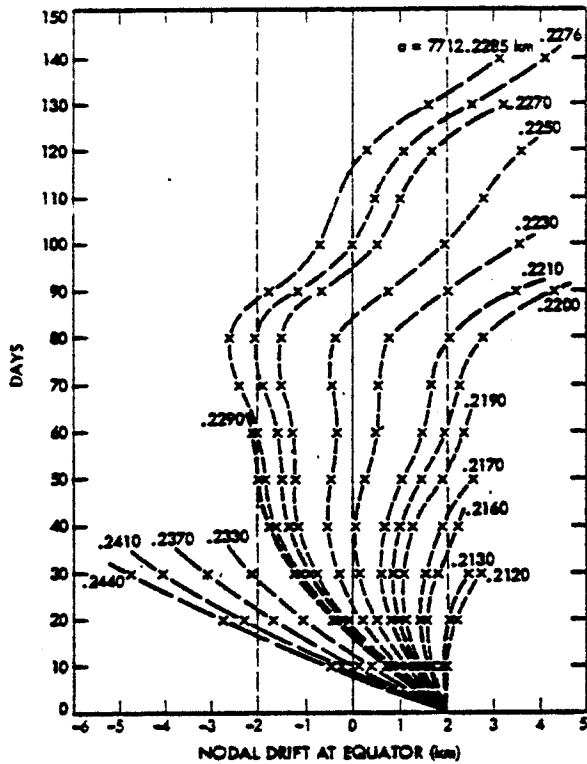


Figure 6. "S" Curves (right limit)  $\pm 2$  km Deadband

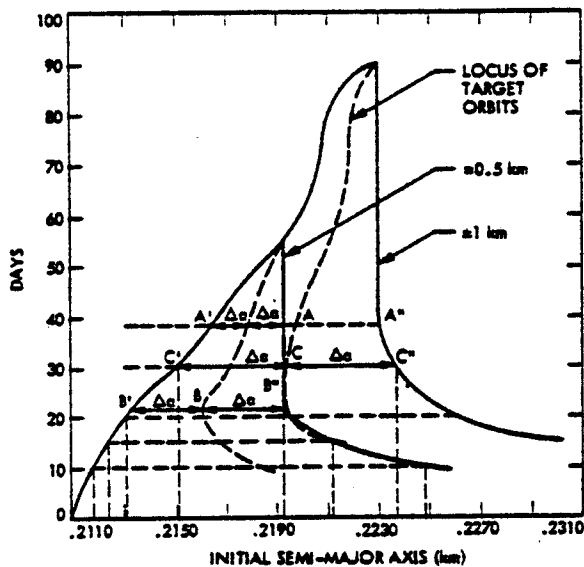


Figure 7. Greatest Lower Bound of Maneuver Period vs. Initial Semimajor Axis

is reached, an instantaneous jump (vertical drop or discontinuity) corresponding to the switch from the right boundary to the left boundary (tangency point of best orbit) takes place, after which, further increases in  $a$ , would yield diminishing values of crossing times on the left boundary.

For the case of the  $\pm 1$  km deadband, there

exists a maximum time of 38 days for which the two extreme orbits yield the same crossing time. The target orbit is presented by point A, midpoint between A' and A'' representing the two extreme orbits.  $\Delta a = A'A = AA''$  with lower equal crossing times always possible for larger values of  $\Delta a$  due to larger values of the fixed execution errors.

In the absence of any orbit determination uncertainties on the premaneuver semimajor axis, there exists a direct relationship between  $\sigma_{\Delta a}$  and  $\sigma_{ex}$ , these values being in reality 3 $\sigma$  values,

$$\sigma_{\Delta a} = K\sigma_{ex} \quad (4.1)$$

In order to determine the value of K which is weakly dependent on the deadband value and the maneuver period, equal crossing times are considered for each equatorial constraint value starting with the highest equal crossing time, read from Figure 7 and 8.

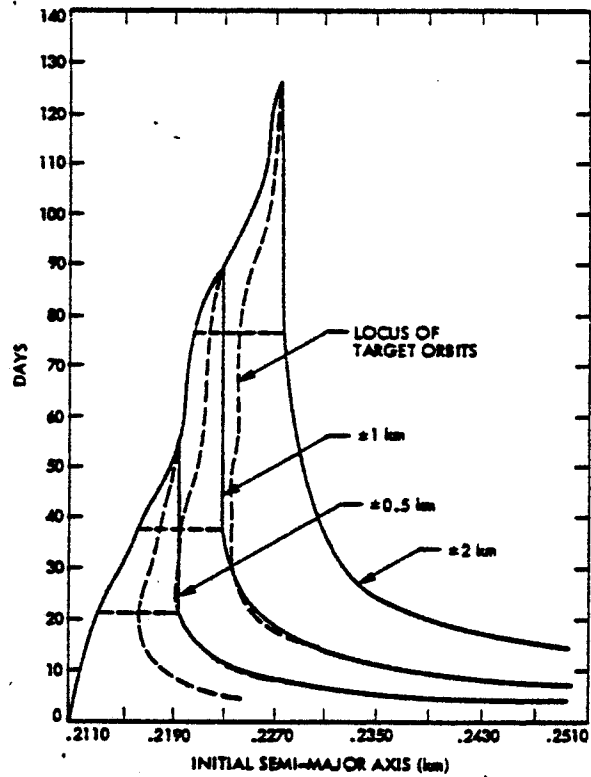


Figure 8. Maneuver Period vs. Initial Semimajor Axis for Given Equatorial Constraint

For example, for the  $\pm 1$  km deadband:

a. Period = 38 days  $\leftarrow$

$$a_{min} = 7712.2165 \text{ km} \quad a_{target}$$

$$a_{max} = 7712.2230 \text{ km} \\ = 7712.2197 \text{ km}$$

b. P = 30 days  $\leftarrow$

$$a_{min} = 7712.2150 \text{ km} \quad a_{target}$$

$$a_{max} = 7712.2237 \text{ km}$$

$$= 7712.2193 \text{ km}$$

c. P = 20 days -

$$a_{min} = 7712.2130 \text{ km}$$

$$a_{max} = 7712.2261 \text{ km} \quad a_{target}$$

$$= 7712.2195 \text{ km}$$

Starting with a premaneuver  $a_{initial} < a_{target}$  and  $e$  initial, and targeting to  $a_{target}$  and  $e_{target} = 0$  to achieve a circular orbit, the transfer solutions are of the nondegenerate type and  $\Delta V_1 =$

$$-\frac{na_{init}}{4} \left( \Delta e - \frac{\Delta a}{a_{init}} \right) \text{ and } \Delta V_2 = -\frac{na_{init}}{4} \left( \Delta e + \frac{\Delta a}{a} \right)$$

with  $\Delta e$  negative and a positive, so that  $\Delta V_2 - \Delta V_1 = \frac{n}{2} \Delta a_{target}$  where  $\Delta a_{target} = a_{target} - a_{initial}$ . On the other hand, the execution errors  $\sigma_{ex}$  are such that the largest achieved  $a_{max}$  corresponds to  $\Delta a_{ach} = a_{max} - a_{init}$  with

$$\Delta a_{ach} = \frac{2(\Delta V_1 + \sigma_{ex})C_{\theta_1} + 2(\Delta V_2 - \sigma_{ex})C_{\theta_2}}{n} \quad (4.2)$$

where  $\theta_1 = 0$  and  $\theta_2 = \pi$  are the impulse locations and  $n$ , the mean motion of the initial premaneuver orbit. Therefore,

$$\Delta a_{ach} = \frac{2}{n} [-(\Delta V_2 - \Delta V_1) + 2\sigma_{ex}] = \Delta a_{target} + \frac{4\sigma_{ex}}{n}$$

$$\sigma_{ex} = \frac{n}{4} (a_{max} - a_{target}) = \frac{n}{4} \sigma_{\Delta a} \quad (4.3)$$

$$K = \frac{\sigma_{\Delta a}}{\sigma_{ex}} = \frac{4}{n} = 4.29 \text{ s/mm/s} \quad (4.4)$$

where  $n = (u/a_{init}^3)^{1/2}$  and  $a_{init} = 7712 \text{ km}$  because of the small amount of semimajor axis decay.

With the value of  $K$  determined by (4.4), the execution errors and the orbit determination uncertainties can be RSS'ed by (4.5) below:

$$\sigma_{\Delta a}^2 = K^2 \sigma_{ex}^2 + \sigma_{OD}^2 \quad (4.5)$$

For a given deadband value,  $\sigma_{\Delta a}$  can be calculated from (4.5) for different values of  $\sigma_{ex}$  and  $\sigma_{OD}$  (Tables 2, 3 and 4). Three levels of  $\sigma_{OD} = 1, 2, 3 \text{ m}$  and three levels of  $\sigma_{ex} = 0.5, 1$  and  $1.5 \text{ mm/s}$  are considered in these tables.

For each value of  $\sigma_{\Delta a}$ , the corresponding maneuver period can be read directly from Figures 7 and 8. For example, for the  $\pm 1 \text{ km}$  deadband, a  $\sigma_{\Delta a}$  corresponding to a given set  $(\sigma_{ex}, \sigma_{OD})$  is shown by  $CC' = C'C = \sigma_{\Delta a}$ ; the target is given directly by the abscissa of point  $C$  and the minimum maneuver period by its ordinate. Inversely for a given minimum maneuver period imposed by the mission planners,  $\sigma_{\Delta a}$  is read from Figure 7 or 8, and

Equation (4.5) used to plot the ellipse in the  $(\sigma_{ex}, \sigma_{OD})$  space. Figures 9 and 10 represent the  $\pm 1 \text{ km}$  and  $\pm 2 \text{ km}$  deadbands and show some ellipses of equal minimum maneuver period. In Figure 9, a minimum maneuver period of 30 days is possible with  $\sigma_{OD} = 0 \text{ m}$  and  $\sigma_{ex} = 1 \text{ mm/s}$  or less while for a  $\sigma_{OD} = 2 \text{ m}$ ,  $\sigma_{ex}$  should be less than  $0.9 \text{ mm/s}$ . Any  $(\sigma_{ex}, \sigma_{OD})$  inside the ellipse satisfies the minimum period requirements.

#### Tables of $\sigma_{\Delta a}$

Table 2.  $\pm 0.5 \text{ km}$  Equatorial Constraint

$\sigma_{ex}(\text{mm/s}) \backslash \sigma_{OD}(\text{m})$	1	2	3
0.5	2.368 (28)	2.934 (24)	3.689 (18)
1.0	4.409 (15)	4.737 (14)	5.238 (12.5)
1.5	6.518 (10)	6.744 (9.5)	7.105 (9)

Table 3.  $\pm 1 \text{ km}$  Equatorial Constraint

$\sigma_{ex}(\text{mm/s}) \backslash \sigma_{OD}(\text{m})$	1	2	3
0.5	2.369 (50)	2.912 (44)	3.671 (34)
1.0	4.350 (30)	4.739 (28)	5.189 (25)
1.5	6.429 (20)	6.658 (19)	7.024 (18.5)

Table 4.  $\pm 2 \text{ km}$  Equatorial Constraint

$\sigma_{ex}(\text{mm/s}) \backslash \sigma_{OD}(\text{m})$	1	2	3
0.5	2.367 (90)	2.933 (85)	3.688 (70)
1.0	4.406 (57)	4.734 (55)	5.235 (52)
1.5	6.513 (41)	6.740 (40)	7.101 (38)

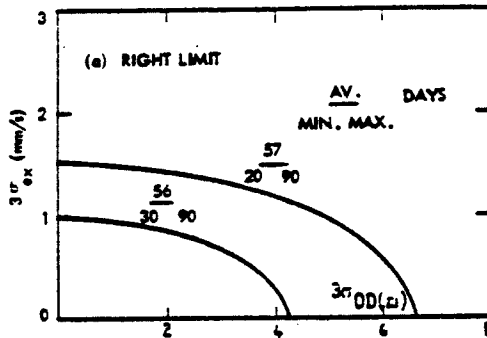


Figure 9. Maneuver Tradeoffs (+1 km constraint)

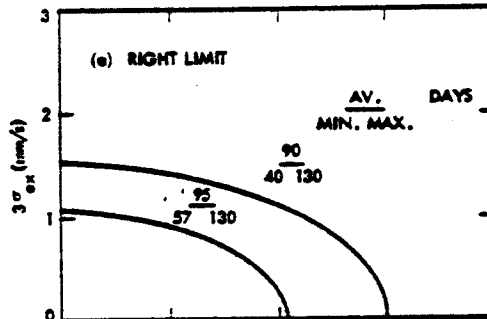


Figure 10. Maneuver Tradeoffs (+2 km constraints)

**V. Orbit Sustainance Maneuver Design:  
Left End Violation**

In the previous section, for the  $\pm 1$  km dead-band, a minimum maneuver period of 30 days with  $\sigma_{ex} = 1$  mm/s and  $\sigma_{OD} = 2$  m was achieved by targeting the spacecraft to the circular orbit  $a = 7712.2193$  km. With the uncertainties listed above, the final achieved orbit will lie between the two bounds  $a = 7712.2237$  km and  $a = 7712.2150$  km, the target orbit being chosen in such a way that these two bounds violate the deadband at the same time (30 days), the highest orbit crossing the left end with the lowest orbit crossing the right end.

Figure 11 shows how these three orbits drift starting from the common right end, with the ideal orbit  $a = 7712.2230$  km staying for the longest time of 90 days inside the deadband. All achieved orbits whose semimajor axis lie between 7712.2150 km and 7712.2230 km will violate the right end after a time  $30 < T < 90$  days, while all achieved orbits whose semimajor axis lie between 7712.2230 and 7712.2237 will necessarily violate the left end. In the case of the left end violation, a re-targeting maneuver to 7712.2193 km would move the node further to the left and is, therefore, inadequate from a design point of view. In this case, a different target orbit must be chosen to remain inside the deadband. The ideal orbit to target the spacecraft at point A (Figure 11) is such that it drifts to the right, starting tangentially to the  $-1$  km end and crossing the right end after the longest possible time.

This orbit with  $a = 7712.2110$  km stays for some 42 days inside the deadband; however, the consideration of fixed magnitude execution errors and OD (orbit determination) uncertainties requires the selection of a target orbit such that with the worst combined uncertainty on the semimajor

axis the ideal orbit 7712.2110 km is never surpassed. Equation (4.5) can be used to determine  $\sigma_{\Delta a}$  with  $K = \bar{n}$  and where  $n$  is the mean motion of the premaneuver orbit at Point A. The orbit elements at A are obtained by letting the circular orbit 7712.2237 km decay for 30 days;  $a_{30} = 7712.2116$  km and  $e_{30} = .2151 \cdot 10^{-3}$  so that  $n = (\mu/a_{30})^{1/2} = .000932183$  rad/s and  $K = 4.298$  m/mm/s. Table 5 shows values of  $\sigma_{\Delta a}$  as a function of  $\sigma_{ex}$  and  $\sigma_{OD}$  using Equation (4.5).

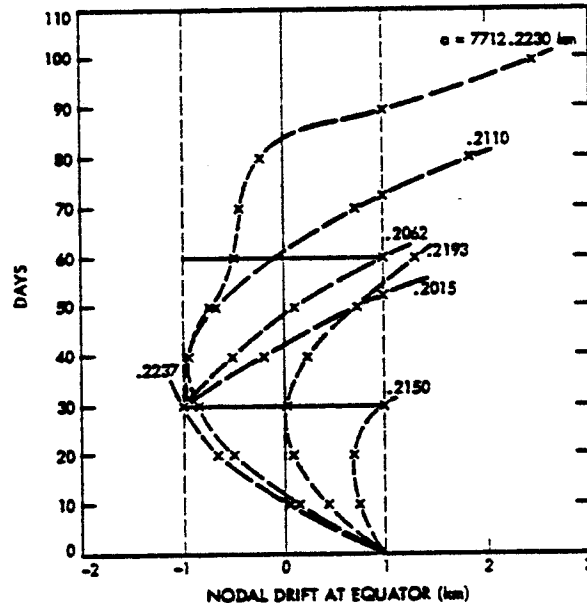


Figure 11. Maneuver Strategy From Left Limit

Table 5. Table of  $\sigma_{\Delta a}$  (m)

$\sigma_{OD}$ (m)	1	2	3	4
$\sigma_{ex}$ (mm/s)				
.5	2.3702	2.9356	3.8903	4.5407
1.0	4.4128	4.7405	5.2415	5.8714
2.0	8.6539	8.8256	9.1044	9.4811

Figures 12 and 13 are used to plot Figure 14, which shows the right end crossing time as a function of initial semimajor axis, for different values of the deadband, namely  $\pm 0.5$  km,  $\pm 1$  km and  $\pm 2$  km. Starting from 7712.2110 km, the drift pattern of several orbits is shown, and the time that each orbit takes before violating the right and is read directly from Figures 12 and 13. For a given  $\sigma_{\Delta a} = f(\sigma_{ex}, \sigma_{OD})$ , the target orbit and the lowest bound are given, respectively, by  $a = 7712.2110 - \sigma_{\Delta a}$  and  $a = 7712.2110 - 2\sigma_{\Delta a}$ .

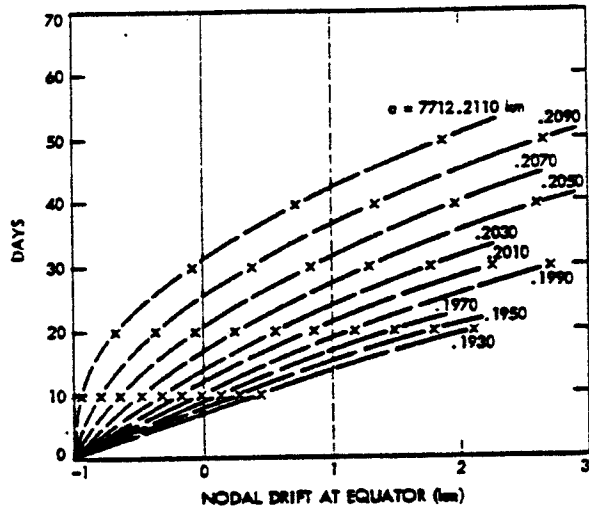


Figure 12. "S" Curves (left limit)  $\pm 1$  km Deadband

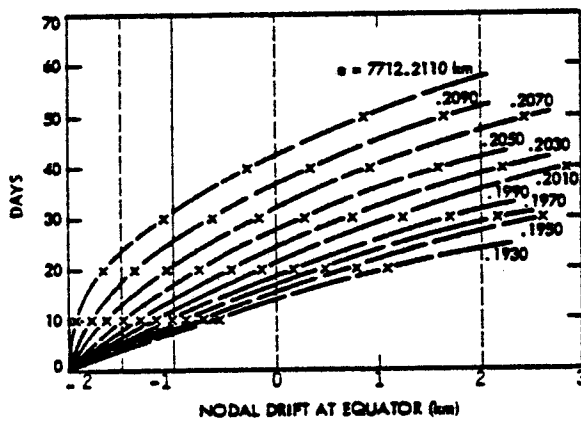


Figure 13. "S" Curves (left limit)  $\pm 2$  km Deadband

Figure 14 then shows the corresponding average and minimum maneuver periods, with the maximum period of 42 days achieved by the highest bound of 7712.2110 km. These orbits are also shown in Figure 11 for  $\sigma_{ex} = 1$  mm/s and  $\sigma_{OD} = 2$  m. Finally, Figures 15 and 16 display ellipses of equal maneuver period, as in the previous section, with each ellipse in the  $(\sigma_{ex}, \sigma_{OD})$  space, associated with three numbers, namely the minimum, average (underlined), and maximum periods. For example, for the  $\pm 1$  km deadband,  $\sigma_{ex} = 1$  mm/s and  $\sigma_{OD} = 2$  m would result in maneuvers with an average period of 30 days but with a most severe minimum of 22 days.

Tables 6 and 7 show the target orbits as a function of  $(\sigma_{ex}, \sigma_{OD})$  and gives also the associated three maneuver periods mentioned above. These periods are slightly lower than the ones corresponding to the target orbits of the previous section for the same  $(\sigma_{ex}, \sigma_{OD})$  combinations.

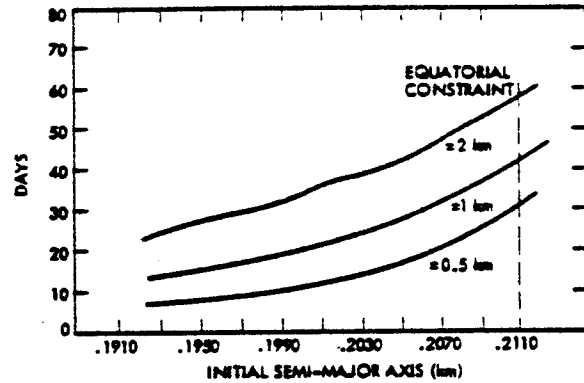


Figure 14. Maneuver Period vs. Initial Semimajor Axis for Different Nodal Constraint Levels

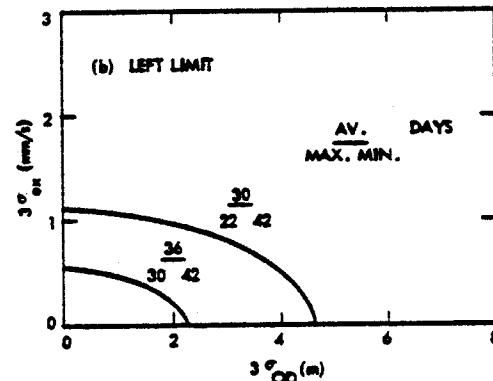


Figure 15. Maneuver Tradeoffs ( $\pm 1$  km Constraint)

Table 6. Target Orbit and Maneuver Period for  $\pm 1$  km Equatorial Constraint

$\sigma_{ex}$ (mm/s)	$\sigma_{OD}$ (m)	1	2	3	4
.5		7712.2086	7712.2080	7712.2073	7712.2064
		30 <u>36</u> 42	28 <u>34</u> 42	25 <u>32.5</u> 42	22.5 <u>30.5</u> 42
1.0		7712.2065	7712.2062	7712.2057	7712.2051
		23 <u>30.5</u> 42	22 <u>30</u> 42	20.5 <u>29</u> 42	19 <u>27.5</u> 42
2.0		7712.2023	7712.2021	7712.2019	7712.2015
		14.5 <u>23</u> 42	14 <u>22.5</u> 42	14 <u>22.3</u> 42	13.5 <u>22</u> 42

It is, therefore, possible to control the drift of the repeat ascending node by using the dual targeting strategy presented in the last two sections. There are, therefore, two target orbits that must be taken into account according to whether the transfer is started from the left or right ends of the deadband.

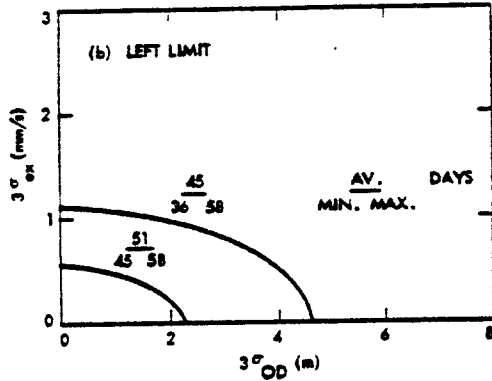


Figure 16. Maneuver Tradeoffs (+2 km Constraint)

Table 7. Target Orbit and Maneuver Period for +2 km Equatorial Constraint

$\sigma_{OD}$ (m)	1	2	3	4
$\sigma_{ex}$ (mm/s)	7712.2086	7712.2080	7712.2073	7712.2064
.5	45 $\frac{51}{45}$ 58	42.5 $\frac{50}{45}$ 58	40 $\frac{48}{45}$ 58	37 $\frac{45.5}{45}$ 58
1.0	7712.2065	7712.2062	7712.2057	7712.2051
	37.5 $\frac{46}{45}$ 58	36.5 $\frac{45}{45}$ 58	34.5 $\frac{43.5}{45}$ 58	32 $\frac{42.5}{45}$ 58
2.0	7712.2023	7712.2021	7712.2019	7712.2015
	25 $\frac{38}{45}$ 58	24.5 $\frac{37.5}{45}$ 58	24 $\frac{37}{45}$ 58	23 $\frac{36.5}{45}$ 58

### Conclusion

This paper shows the combined effect of the maneuver execution errors and orbit determination uncertainties on the maneuver period of the orbit sustenance phase of the TOPEX spacecraft for different equatorial nodal deadband values. Ellipses of equal minimum and average maneuver times are presented in the  $(3\sigma_{ex}, 3\sigma_{OD})$  space corresponding to the different deadbands enabling the determination of the appropriate combination of  $3\sigma_{ex}$  and  $3\sigma_{OD}$  that guarantees a mission required maneuver period for a given equatorial deadband, through interpolation.

During each targeting maneuver, the orbit is circularized even though eccentricity is not a factor affecting the nodal drift, because no savings in fuel are possible by delaying the circularization. This is due to the linear growth of  $e$  with time and also to the fact that the changes in the eccentricity are much larger than the relative changes in the semimajor axis, which decays only by 60 m in 400 days. Therefore, the total  $\Delta V = 50$  m/s needed for the entire five years duration of the mission is independent of maneuver frequency.

Finally, it is shown that a maneuver period of 30 days or more is only possible with  $\sigma_{ex} < 1$  mm/s combined with  $\sigma_{OD} < 2$  m for a deadband of  $\pm 1$  km. A statistical analysis based on the Monte Carlo sampling technique should now be possible to carry

out, in order to obtain a more precise evaluation of the statistical maneuver periods.

### Appendix A: Linearized Optimal Transfer Between Close Coplanar Near-Circular Orbits

The transfer solutions used to design the targeting strategies presented in this paper are drawn from the linear theory of optimal transfer between close coplanar near-circular orbits described briefly below.

#### I. General Analysis

Let  $x$  represent the direction of periape in a frame centered at Earth and  $y$  complete the system. If a small  $\Delta V$  is applied in the direction of the unit vector  $\hat{s}$  at position  $\theta$  measured from the  $x$ -axis of the reference, then the changes experienced by the orbit elements (semimajor axis  $a$ , and eccentricity vector  $\vec{e}$ ) are

$$\frac{\Delta a}{a} = 2\tau \beta_e \quad (A-1)$$

$$\Delta e_x = \tau(\beta_r s_\theta + 2\beta_\theta c_\theta) \quad (A-2)$$

$$\Delta e_y = \tau(-\beta_r c_\theta + 2\beta_\theta s_\theta) \quad (A-3)$$

$\tau = \frac{\Delta V}{na}$  represents the normalized  $\Delta V$  with  $n$  the mean motion of the spacecraft and  $\beta_r = s_\theta$  and  $\beta_\theta = c_\theta$ , the components of the unit vector  $\hat{s}$  along the radial and 90° ahead directions in the orbit plane. This reference frame attached to the spacecraft is the Euler-Hill frame and  $\theta$  is the angle between  $\hat{s}$  and its  $\beta_\theta$  component. Equations (A-1)-(A-3) can be derived by using, for example, the theory of the displacement of the vacant focus due to a small impulsive  $\Delta V$ . In a more compact form, these equations, linear in  $\tau$ , can be written as

$$\frac{\vec{e}}{\tau} = \begin{pmatrix} \frac{\Delta a}{a}/\tau \\ \Delta e_x/\tau \\ \Delta e_y/\tau \end{pmatrix} = \sum_j M(\theta_j) \hat{\beta}_j \quad (A-4)$$

$$= \begin{pmatrix} 0 & 2 \\ s_\theta & 2c_\theta \\ -c_\theta & 2s_\theta \end{pmatrix} \begin{pmatrix} \beta_r \\ \beta_\theta \end{pmatrix}$$

A multi-impulse maneuver (maximum of three for this problem) is optimal if and only if there exists a Lagrange multiplier vector  $\vec{\lambda}^T = (\lambda_a, \lambda_e, \lambda_e)$  such that for each combination of impulse

location and direction  $(\theta_j, \beta_j)$  used to achieve a transfer, the Hamiltonian below is maximum.

$$H = \vec{\lambda}^T M(\theta) \hat{\beta} \quad (A-5)$$

The maximization of  $H$  with respect to  $\hat{\beta}$  requires that  $\hat{\beta}$  be parallel to  $M^T(\theta) \vec{\lambda} = \vec{\lambda}_y$ , Lawden's primer vector, which is now a function of  $\theta$  alone. The

impulsive  $\Delta V$ 's are then applied at positions  $\theta$  that maximize  $|\dot{\lambda}_V|$  along the  $\dot{\lambda}_V$  orientation.

### II. Evolution of the Primer Vector $\dot{\lambda}_V$

$\dot{\lambda}_V$  is a periodic function in  $\theta$  and its two components in the  $\hat{r}$  and  $\hat{\theta}$  rotating frame (Euler-Hill) are given by

$$\begin{aligned} \dot{\lambda}_V &= \begin{pmatrix} \dot{\lambda}_r \\ \dot{\lambda}_\theta \end{pmatrix} = M^T(\theta) \dot{\lambda} = \lambda_a \begin{pmatrix} 0 \\ 2 \end{pmatrix} \\ &+ \lambda_{e_x} \begin{pmatrix} s_\theta \\ 2c_\theta \end{pmatrix} + \lambda_{e_y} \begin{pmatrix} -c_\theta \\ 2s_\theta \end{pmatrix} \end{aligned}$$

Let  $\lambda_{e_x} = \mu s_{\theta_0}$  and  $\lambda_{e_y} = -\mu c_{\theta_0}$  with

$$\theta_0 = \tan^{-1} \left( -\frac{\lambda_{e_x}}{\lambda_{e_y}} \right) \quad (A-7)$$

Then

$$\dot{\lambda}_r = \mu c_{\theta - \theta_0} \quad (A-8)$$

$$\dot{\lambda}_\theta = 2\lambda_a - 2\mu s_{\theta - \theta_0} \quad (A-9)$$

Several cases can now be considered

1)  $\mu \neq 0$

$$\lambda_a = 0$$

Equations (A-8) and (A-9) describe a two to one ellipse in the  $(\lambda_r, \lambda_\theta)$  frame (Figure A-1) as  $\theta - \theta_0$  is allowed to increase from 0 to  $2\pi$ . The ellipse being centered at the origin,  $|\dot{\lambda}_V|$  is maximum when  $\lambda_\theta = 2\mu$ ,  $\lambda_r = 0$ , corresponding to  $\theta - \theta_0 = \pm\pi/2$ . The two impulses corresponding to the two equal maxima of  $|\dot{\lambda}_V|$  are, therefore, purely tangential and separated by  $180^\circ$  in true anomaly.

2)  $\mu = 0$

$$\lambda_a \neq 0$$

Then Equations (A-8) and (A-9) reduce to  $\dot{\lambda}_r = 0$  and  $\dot{\lambda}_\theta = 2\lambda_a$  indicating that  $|\dot{\lambda}_V|$  is independent of angular position  $\theta - \theta_0$  with equal preference for all points on the orbit as an impulse location. The thrust is again applied tangentially, since  $\dot{\lambda}_r = 0$  and  $|\dot{\lambda}_V| = 2\lambda_a$  corresponding to the two points along the  $\lambda_\theta$  axis of the  $\lambda_r, \lambda_\theta$  frame (Figure A-1).

3)  $\mu \neq 0$

$$\lambda_a \neq 0$$

Equations (A-8) and (A-9) describe a two to one ellipse as in the first case, but with its center at  $(0, 2\lambda_a)$  in the  $(\lambda_r, \lambda_\theta)$  space.  $|\dot{\lambda}_V|$  reaches its only maximum at  $\lambda_r = 0$ ,  $\lambda_\theta = 2(\mu - \lambda_a)$  when  $|\theta - \theta_0| = \pi/2$ . The impulse is applied in the  $\theta$

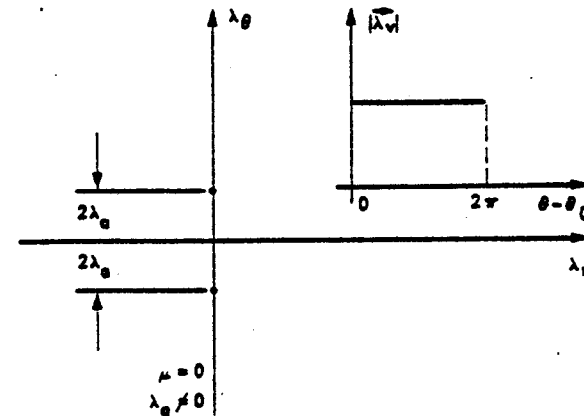
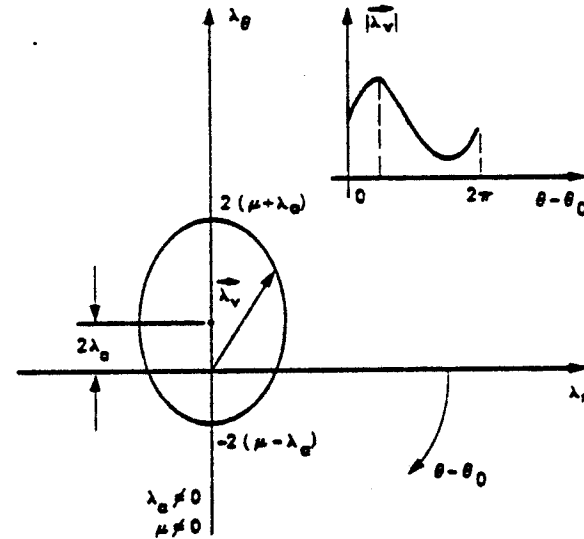
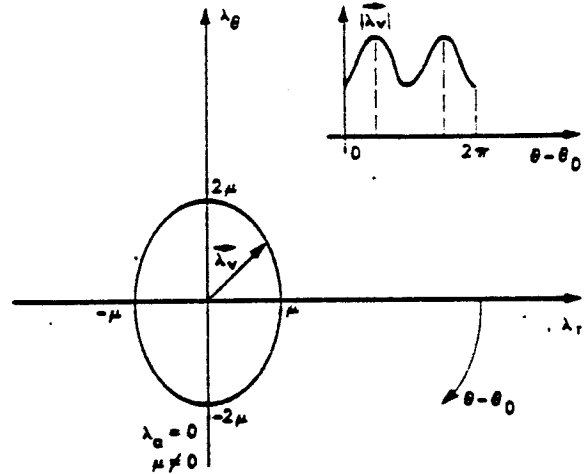


Figure A1. Evolution of Primer Vector

direction (tangential) at position  $\theta - \theta_0 = -\pi/2$  if  $\lambda_E > 0$  and for  $\lambda_E = 2u + 2\lambda_A > 0$  or at position  $\theta - \theta_0 = \pi/2$  if  $\lambda_E < 0$  and for  $\lambda_E = -2u + 2\lambda_A < 0$ .

### III. Optimal Solutions via Contensou's Spool

The set of points  $(\frac{\Delta a}{a}/\tau, \frac{\Delta e_x}{\tau}, \frac{\Delta e_y}{\tau})$  can be resolved

into a convex mixture of points on a surface called after the French mathematician Pierre Contensou (Contensou's spool) consisting of all single-impulse points given by (A-10) and shown in Figure A-2.

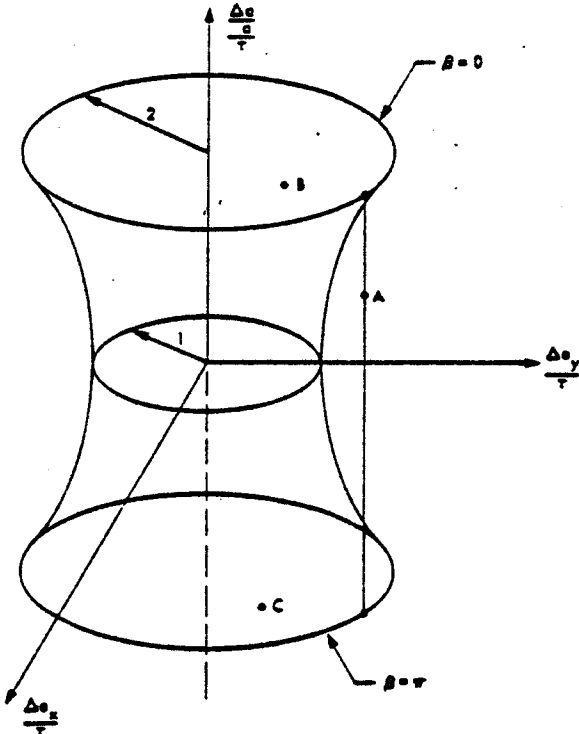


Figure A2. Contensou's Spool. Minimum  $\Delta V$  Transfer Between Coplanar Near-Circular Orbit

$$\left. \begin{aligned} \frac{\Delta a}{a}/\tau &= 2C_B \\ \frac{\Delta e_x}{\tau} &= s_B s_\theta + 2C_B C_\theta \\ \frac{\Delta e_y}{\tau} &= -s_B C_\theta + 2C_B s_\theta \end{aligned} \right\} \quad (A-10)$$

Given  $\frac{\Delta a}{a}$ ,  $\Delta e_x$ , and  $\Delta e_y$ , the necessary and sufficient condition for the minimization of  $\tau$  (minimum-impulse) is that the point  $(\frac{\Delta a}{a}/\tau, \frac{\Delta e_x}{\tau}, \frac{\Delta e_y}{\tau})$  lie on the convex hull of Contensou's spool. The upper circle of radius 2 (Figure A-2) corresponds to  $\frac{\Delta a}{a}/\tau = 2$  and  $\beta = 0$  (accelerating  $\Delta V$ ) while the lower circle of the same size corresponds to  $\frac{\Delta a}{a}/\tau = -2$  and  $\beta = \pi$  (decelerating  $\Delta V$ ). By definition of (A-1); the reachable state  $\frac{\Delta a}{a}/\tau$  is convex and every orbit transfer is a convex mixture of the two

cases just described, namely with  $\beta = 0$  and  $\beta = \pi$ .

There are two types of optimal transfers in this linear theory.

#### Type I - Nondegenerate:

It is the Hohmann transfer and corresponds to a point like A on the cylindrical hull of Contensou's spool (Figure A-2) and consists of a combination of two impulses  $\beta_1 = 0$  and  $\beta_2 = \pi$ , respectively. The firing locations are separated by  $\pi$  because  $\dot{X}$  is periodic in  $\theta$  with period  $\pi$ . Equations (A-10) reduce to

$$\left. \begin{aligned} \frac{\Delta a}{a} &= \frac{2}{na} (\Delta V_1 - \Delta V_2) \\ \Delta e_x &= \frac{2}{na} C_{\theta_1} (\Delta V_1 + \Delta V_2) \\ \Delta e_y &= \frac{2}{na} s_{\theta_2} (\Delta V_1 + \Delta V_2) \end{aligned} \right\} \quad (A-11)$$

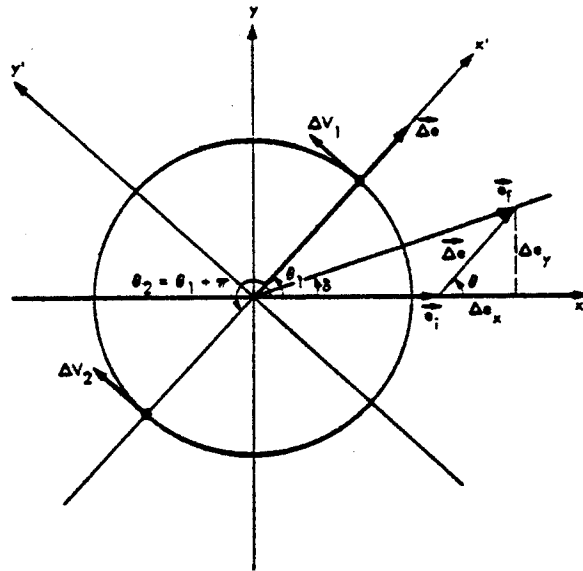


Figure A3. Firing Geometry

$\theta_1$  is the location of the first impulse and  $\theta_2 = \theta_1 + \pi$  the location of the second impulse. The last two equations of (A-11) give  $\tan \theta_1 = \frac{\Delta e_y}{\Delta e_x}$ ,

indicating that the impulse locations are along a line parallel to  $\Delta e$  (Figure A-3), since  $\Delta e$  is itself inclined at an angle  $\theta$  with respect to the

x-axis with  $\tan \theta = \frac{\Delta e_y}{\Delta e_x}$ . Therefore,  $\theta_1 = \theta$ . In

order to solve for the two  $\Delta V$ 's, advantage is taken of the rotational symmetry of Contensou's spool by a rotation of the reference frame  $(x, y)$  through

an angle  $\theta = \tan^{-1} \frac{\Delta e_y}{\Delta e_x}$ , aligning the new  $x'$ -axis

with the  $\Delta e$  vector. The magnitude of  $\Delta e$  needs to be considered then instead of the set  $\Delta e_x, \Delta e_y$  allowing, thereby, the resolution of the impulsive  $\Delta V$ 's by reducing (A-11) to the system below

$$\left. \begin{aligned} \frac{\Delta a}{a} &= \frac{2}{na} (\Delta V_1 - \Delta V_2) \\ \Delta e &= \frac{2}{na} (\Delta V_1 + \Delta V_2) \end{aligned} \right\} \quad (A-12)$$

Here, the set  $(\frac{\Delta a}{a}, \Delta e_x, \Delta e_y)$  has been reduced to the set  $(\frac{\Delta a}{a}, \Delta e, 0)$  where

$$\Delta e = \text{sgn}(e_f - e_1) (\Delta e_x^2 + \Delta e_y^2)^{1/2}$$

$$\theta = \tan^{-1} \left( \frac{\Delta e_y}{\Delta e_x} \right)$$

These solutions of Type I correspond to  $\Delta e^2 > (\frac{\Delta a}{a})^2$  and the overall  $\Delta V$  sum is dependent only on  $|\Delta e|$  so that  $\Delta V_1 + \Delta V_2 = \frac{na}{2} |\Delta e|$ .

#### Type II - Singular

These transfers correspond to points like B or C (Figure A-2) which are achieved by a convex mixture of points lying on the upper or lower circumference of Contensou's spool, obtainable in an infinite number of combinations all with  $\beta = 0$  (point B) or  $\beta = \pi$  (point C), according to whether  $\Delta a > 0$  or  $\Delta a < 0$ . The Hamiltonian being flat, all points on the orbit are candidates for an impulsive location. Two-impulse solutions are constructed by locating point G along the  $\Delta e$  direction and such that (Figure A-4)

$$\vec{FG} = \frac{\vec{\Delta e}}{(\Delta a/a)} \quad (A-13)$$

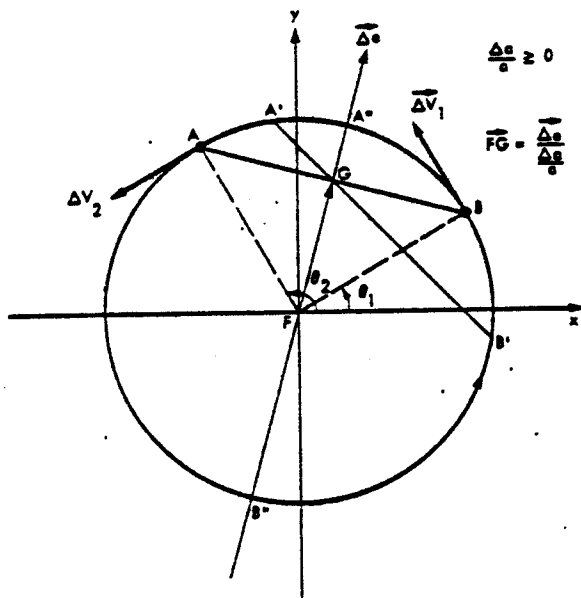


Figure A4. Singular-Case Min. Spacing Between  $\Delta V$ 's

F being the center of the Earth, any line passing through G intersects the orbit in two points like A' and B', which represent the firing locations.

When the line is along A'B", the impulses are  $180^\circ$  apart and are of the Hohmann type. The angular separation between the two impulses is minimum when AB is perpendicular to FG with

$$(\Delta \theta)_{\min} = 2 \cos^{-1} \left[ \frac{\Delta e}{(\Delta a/a)} \right]$$

In this case the V's have equal magnitude  $\Delta V_1 = \Delta V_2 = \frac{na}{4} \frac{|\Delta a|}{a}$  while for any other orientation of line AB, the V's are such that point G is their "center of mass" along AB. The solutions of Type II correspond to  $\Delta e^2 < (\frac{\Delta a}{a})^2$  and the overall  $\Delta V$  sum is dependent only on  $|\frac{\Delta a}{a}|$ , such as  $\Delta V_1 + \Delta V_2 = \frac{na}{2} \frac{|\Delta a|}{a}$ .

Figure A-5 shows how the  $(\Delta e, \frac{\Delta a}{a})$  space is partitioned into Type I and Type II zones. The flow chart diagram presented in Figure (A-6) branches out into two main parts, according to whether  $\Delta e^2 > (\frac{\Delta a}{a})^2$  (Type I),  $\Delta e^2 < (\frac{\Delta a}{a})^2$  (Type II). For Type I, and according to the sign of  $\Delta e$ , two solutions are shown for each case because the  $\Delta V$ 's can be applied in either order and achieve the same transfer. For Type II, solutions are shown in the flow chart diagram corresponding to an angular separation of  $180^\circ$  (Hohmann type) both for  $\frac{\Delta a}{a} > 0$  and  $\frac{\Delta a}{a} < 0$ . The chronological order of application of the two impulses being immaterial, the two corresponding solutions are displayed once again.

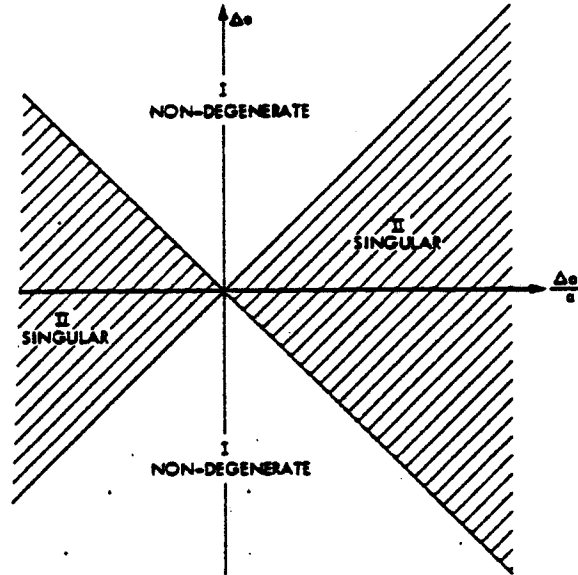


Figure A5. Partition of State Space

For the particular case in which  $\Delta e_x = \Delta e_y = 0$ ,  $\Delta e = 0$  corresponds to a transfer between two concentric circles or two similar, similarly oriented ellipses. The solutions are of the Type II with  $\Delta V_1 = \Delta V_2 = \frac{na}{4} \frac{|\Delta a|}{a}$ . If  $\frac{\Delta a}{a} = 0$ , the solutions are of Type I and the  $\Delta V$ 's are again of equal size  $\Delta V_1 = \Delta V_2 = \frac{na}{4} |\Delta e|$ . If  $|\Delta e| = \frac{|\Delta a|}{a}$ , the orbits intersect tangentially, and the transfer requires only one impulse applied at that intersection point. The two branches of the flow chart diagram yield the same solution. This case

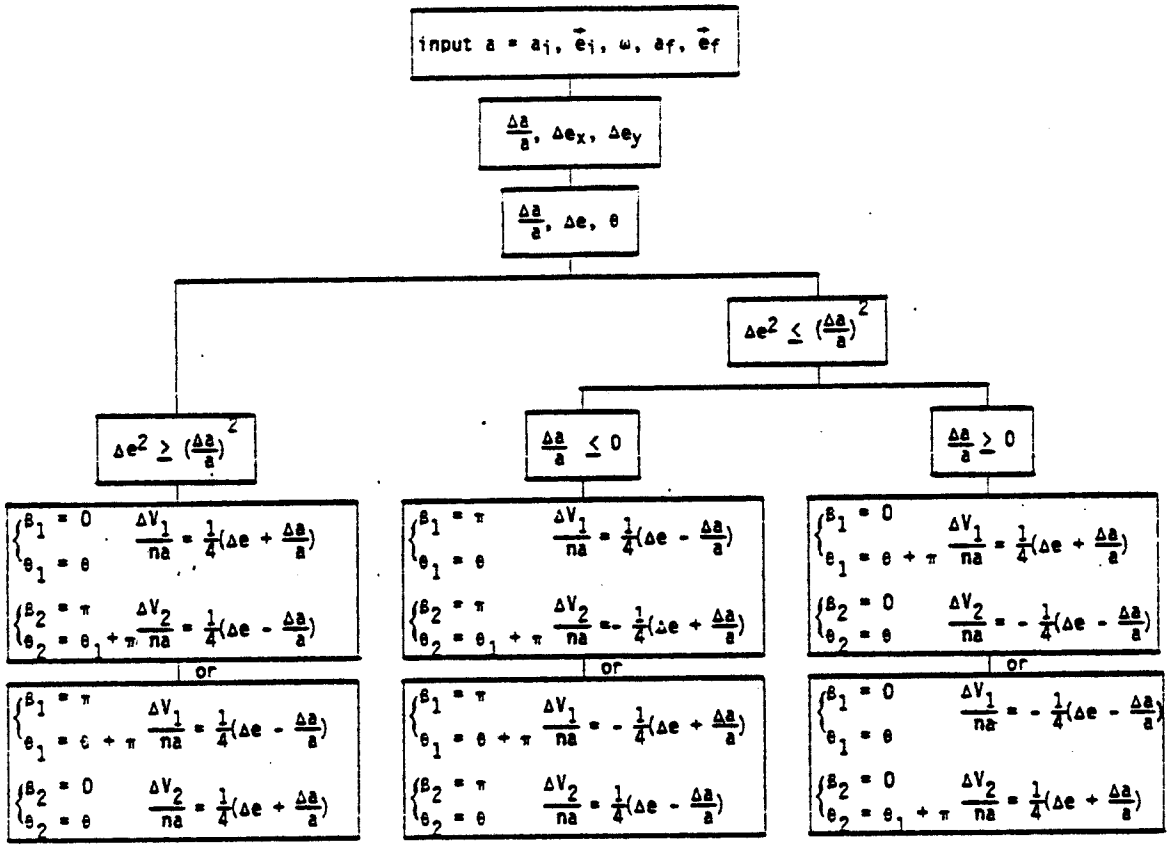


Figure A-6. Transfer Solutions

corresponds to Point G given by (A-13) lying on the orbit and representing the line AB itself which collapses to G.

Appendix B. Relative Motion of Two Close Satellites in Coplanar Near-Circular Orbits

This brief appendix is used to show the dependence of the uncertainty in the semimajor axis on the uncertainties in the radial direction and the forward velocity. The radial uncertainty can be attributed to orbit determination while the velocity error is due to maneuver execution errors.

Let  $(x, y)$  represent the rotating Euler-Hill frame attached to a spacecraft in a nominal circular orbit, with  $x$  along the radial and  $y$  along the velocity error. Let  $\vec{r}(t)$  represent the instantaneous position vector of a second satellite in a close near-circular coplanar orbit with  $\vec{p}(t)$ , its relative position in the rotating frame. At  $t = 0$ ,  $x_0, y_0, \dot{x}_0, \dot{y}_0$  being the components of its relative position and velocity vectors, its relative motion is described by the Euler-Hill Equations (B-1).

$$\left. \begin{aligned} \ddot{x} - 2n\dot{y} - 3n^2x &= 0 \\ \ddot{y} + 2n\dot{x} &= 0 \end{aligned} \right\} \quad (B-1)$$

where  $n = \sqrt{\frac{\mu}{a^3}}$  is the spacecraft mean motion, with  $a$  its orbit semimajor axis. The solution of (B-1) is given below

$$\left. \begin{aligned} x &= \frac{\dot{x}_0}{n} s_{nt} - \left(\frac{2\dot{y}_0}{n} + 3x_0\right) c_{nt} + \left(\frac{2\dot{y}_0}{n} + 4x_0\right) s_{nt} \\ y &= \frac{2\dot{x}_0}{n} c_{nt} + \left(\frac{4\dot{y}_0}{n} + 6x_0\right) s_{nt} + \left(y_0 - \frac{2\dot{x}_0}{n}\right) c_{nt} - (3\dot{y}_0 + 6nx_0)t \end{aligned} \right\} \quad (B-2)$$

For a near-circular orbit it is convenient to replace  $e$  (eccentricity) and  $w$  (argument of perigee), the latter poorly defined by

$$\xi = ec_w \quad (B-3)$$

$$\eta = es_w \quad (B-4)$$

On the other hand, the orbit equation can be expressed in terms of  $\xi$  and  $\eta$ , since

$$r = a(1 - e \cos E) = a(1 - e \cos M) + O(e^2) \quad (B-5)$$

$$= a(1 - \xi c_{nt} - \eta s_{nt}) + O(e^2)$$

where E is the eccentric anomaly, M the mean anomaly, and where

$$E = M + e \sin M + O(e^2)$$

$$M = n(t - t_p)$$

with  $t_p$  representing time at periape.

Equation (B-5) can be used to express the relative change in semimajor axis with  $x = \delta r$ ,

$$\frac{\delta a}{a} = \frac{x}{a} + \delta \xi c_{nt} + \delta \eta s_{nt} \quad (B-6)$$

In order to obtain an expression for  $\delta a$  as a function of relative initial position and velocity,  $\delta \xi$  and  $\delta \eta$  must be expressed first in terms of those same quantities. The angular position  $\theta$  measured from the reference direction is given by

$$\theta = \omega + M + 2e \sin M + O(e^2) \quad (B-7)$$

$$\theta = \theta_0 + nt + 2(\xi c_{nt} - \eta s_{nt}) + O(e^2)$$

where  $\theta_0 = \omega - nt_p$ .

From  $n = \left(\frac{\mu}{a^3}\right)^{1/2} - \delta n = -\frac{3}{2} \frac{n}{a} \delta a$ , so that  $(B-8)$

$$\delta \theta = \delta \theta_0 - \frac{3}{2} \frac{\delta a}{a} nt + 2\delta \xi s_{nt} - 2\delta \eta c_{nt}$$

But since  $y = a\delta\theta$ , Equation (B-8) and (B-2) can be equated to give

$$\delta \xi = \frac{2\dot{y}_0}{na} + \frac{3x_0}{a} \quad (B-9)$$

$$\delta \eta = \frac{-x_0}{na} \quad (B-10)$$

$$\delta a = \frac{2\dot{y}_0}{n} + 4x_0 \quad (B-11)$$

Equation (B-11) can also be obtained by expressing  $y = a\delta\theta$  and using (B-9) and (B-10) above such that

$$\delta a = \frac{2\dot{y}_0}{n} + 4x_0 = \frac{2\dot{y}_0}{n} + 4x_0 \quad (B-12)$$

This equation shows that the uncertainty on the semimajor axis is a function of the uncertainty in the radial direction  $x$  and the uncertainty in the forward velocity  $y$  measured in the Euler-Hill frame.

#### Acknowledgement

The author wishes to express his gratitude to E. Cutting and J. B. Jones for useful discussions and to J. Howard and N. Clinton for the typing of the manuscript.

The research described in this publication was carried out by the Jet Propulsion Laboratory,

California Institute of Technology, under contract with the National Aeronautics and Space Administration.

#### Bibliography

1. Cutting, E., "TOPEX Baseline Orbit Characteristics," JPL Internal Document 312/80.1-174-EC, 9 December 1980.
2. Cutting, E., "SAMDP Study of Long Term Characteristics of TOPEX Baseline Orbit," JPL Internal Document 312/81.1-177-EC, 26 January 1981.
3. Khan, I. R., "Design and Implementation of Models for Satellite Mission Design Program," JPL Internal Document 312/78-54, 13 February 1978.
4. Stewart, R., "Satellite Altimetric Measurements of the Ocean," Report of the TOPEX Science Working Group, JPL Document, 1 March 1981.
5. Schanzle, A., Daus, M., Marechek, G., "Prelaunch Orbital Error Analysis for the TOPEX Satellite," EG&G Washington Analytical Services Center, Inc., Riverdale, MD., February 1981.
6. Contensou, P., "Etude Théorique des Trajectoires Optimales Dans Un Champ De Gravitation: Application A Un Cas D'un Centre Unique," Acta Astronautica, 8, pp. 134-150, 1962.